Article:
WILSON, Sarah and DESSENT, CAROLINE ELIZABETH HELEN (2026) Mapping Molecular Excited States via Relative Ion Yield Photodissociation Spectroscopy. ChemPhysChem. e202500649. ISSN: 1439-4235

https://doi.org/10.1002/cphc.202500649

Author accepted manuscript

Mapping Molecular Excited States via Relative Ion-Yield Photodissociation Spectroscopy

Sarah A. Wilson and Caroline E. H. Dessent*

Department of Chemistry, University of York, Heslington, York, YO10 5DD, UK.

*E-mail: caroline.dessent@york.ac.uk

Abstract

Laser photodissociation spectroscopy of gaseous ions is a widely applicable technique used to investigate the electronic excited states and photochemistry of charged systems ranging from inorganic nanoclusters through to biomolecules. Spectra obtained by this technique provide important benchmarks for theoretical studies of dissociative excited states, and give insight into light-induced fragmentation pathways. In this concept article, we will highlight the advantages of obtaining and analysing photodissociation action spectra in terms of photon-energy dependent *relative ion yield plots*. This new approach to analysing ion photodissociation spectra has been demonstrated by our laboratory over recent years and is based on the photochemical concept of quantum yields. Importantly, relative ion yield analysis allows experimental vertical excitation energies of charged systems to be straightforwardly identified for comparison to theory. The application of relative ion yield analysis also provides greater insight into excited-state decay dynamics than is evident from inspection of individual photofragment action spectra. To provide a suitable introduction to the relative ion yield concept for non-expert readers, we begin the article by reviewing the broader topic of ionic photofragment action spectroscopy. Results from several UV filter molecules are then presented to illustrate the advantages of relative ion yield analysis.

Keywords

Computational Chemistry, Chromophores, Electronic Spectroscopy, Photochemistry, Ion Spectroscopy, Photolysis, Quantum Yield.

Graphical Abstract

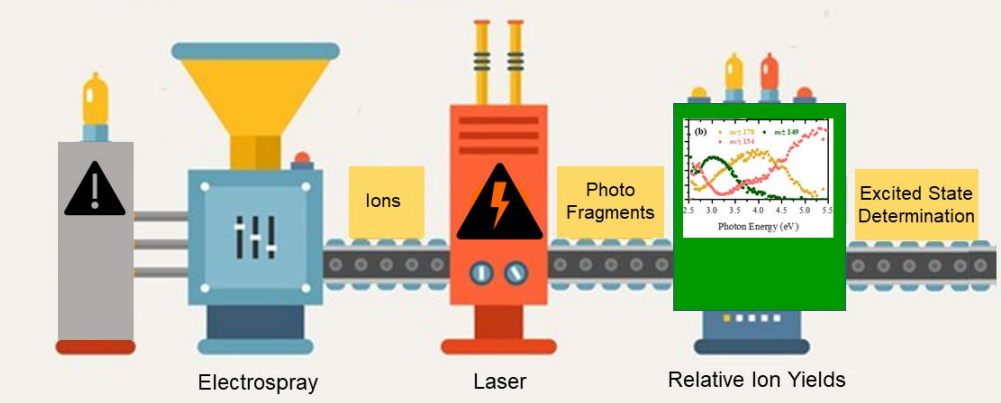

Text for Table of Contents

This concept provides a concise overview of the development of relative ion yield plots from laser photodissociation measurements of gaseous molecular ions. The advantages of relative ion plots for obtaining information on excited states including vertical excitation energies and photochemical decay processes are discussed.

Introduction

A robust understanding of molecular excited states and the reactive pathways that evolve after photoexcitation is fundamental for exploiting light-matter interactions in frontline scientific fields including solar energy conversion, photocatalysis, and organic electronics.[1] Despite their importance, the computation of excited states and dynamics remains one of the key challenges for contemporary theoretical chemistry.[2] To advance progress in this field, the availability of strong benchmarking data from experiment is of key importance. Gas-phase experiments offer many advantages for obtaining high-quality benchmarking data, since measurements are not affected by perturbations from counterions, solvent effects, or the involvement of aggregates.[3–7] Spectral resolution is also typically higher than in solution-phase studies due to reduced thermal congestion.

While many early gas-phase excited state spectroscopy studies were conducted on neutral molecular systems,[4–6] over the last two decades considerable advances have been achieved by performing electronic spectroscopy on ionic species which have been transferred to the gas-phase by electrospray ionization (ESI). The electronic spectroscopy of a plethora of ESI-generated systems have been studied including organic chromophores, large biological molecules and inorganic materials.[8–19]

In measurements of gaseous ions, electronic absorption spectra are generally obtained through photodepletion measurements.[20–22] Although excited states can be identified in the resulting photodepletion spectra, this is not always straightforward. Contributions from overlapping bands, for example, can cancel out over particular wavelength ranges making it challenging to accurately locate the experimental vertical excitation energies (VEEs). In this concept article, we will highlight recent work from our laboratory showing the value of analysing photofragment action spectra in terms of photon-energy dependent *relative ion yield plots*. These plots allow vertical excitation energies to be straightforwardly identified, and hence provide robust benchmarks for advanced computational chemistry. Since the details of photodissociation action spectroscopy of ions may not be familiar to all readers, especially computational and theoretical chemists, we begin by presenting a brief overview of the technique as a basis for understanding the relative ion yield plots.

While the focus of this article is electronic photofragmentation spectroscopy of ions, other gas-phase electronic spectroscopy approaches can be used to characterise electronic excited states and locate experimental VEEs. Combinations of molecular beam sources with high-resolution

lasers, coupled to photoionization detection were extensively used for studying molecules and aggregates.[4–6,23–31] Although these measurements provided exceptional, high-resolution spectral data, experiments were typically performed on volatile molecules that could be readily transferred via supersonic expansion into a molecular beam. This limited the range of molecular systems investigated compared to experiments where precursors are prepared by electrospray. Anion photoelectron spectroscopy offers another, distinctive route to obtaining VEEs of neutral systems, with the caveat that neutral state geometries accessed are those corresponding to the initial anionic geometry.[32–35] We refer the reader to the review of Pereverzev and Roithva for a comparative overview of gas-phase spectroscopy techniques.[36]

Overview of Action Spectroscopy for Gas-Phase Electronic Spectroscopy of Ionic Molecular Systems

The gas-phase offers considerable advantages for performing spectroscopy on molecular systems, but direct absorption spectroscopy is generally not viable as the molecular concentration is too low for observing absorbance.[22] This limitation is present irrespective of the electromagnetic radiation employed, or whether the system under study is uncharged or charged. For the specific case of electrosprayed ions, the number of ions that can be generated is typically around 10^6, so measurement of direct absorption is not experimentally feasible.

Action spectroscopy offers a solution to the non-viability of direct absorption spectroscopy for gas-phase measurements. It allows a spectrum to be obtained by recording the production of a molecular fragment (or an electron) following the resonant absorption of a photon by a molecule or aggregate (cluster). Hence the spectrum is collected by recording an "action" that ensues following photon absorption. Figure 1 provides a schematic overview of the general sequence involved in acquiring action spectra for gaseous ions. In this illustration, which reflects our experimental approach, ions are generated via electrospray ionization (ESI), undergo mass selection (MS1), and interact with the laser source. Photofragments are subsequently separated (MS2) and detected.[37] The use of ESI to generate the gaseous ions of interest means that a very wide range of chemical systems can be studied by this method, subject to the requirement that they are soluble in a polar solvent. (Solute concentrations are ~10^{-6} mol dm^{-3}.)

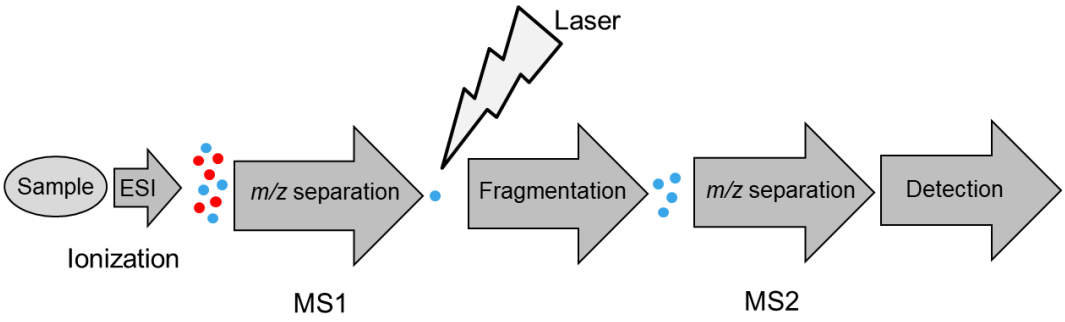

Figure 1: Schematic diagram of a typical action spectroscopy experiment for gaseous ions.

Equation 1 illustrates the action spectroscopy process for a simple cationic molecular cluster, $A{\cdot}B^+$, where the photon is resonant with a vertically accessible excited state of the cluster that is energetically above the dissociation threshold:

$$A{\cdot}B^+ + h\nu \rightarrow A + B^+ \quad [1]$$

Action spectra can then be recorded either via depletion of the precursor ion, $A{\cdot}B^+$, or the production of the photofragment ion, B^+, across a chosen wavelength range. In both cases, mass spectrometric detection is used to measure ion intensity as the photon energy changes. For larger molecular systems, M^+, multiple fragmentation pathways are typically present as depicted by [2a]-[2c] where X^+, Y^+ and Z^+ are different fragment ions and N_1-N_3 are their accompanying neutral fragments:

$$M^+ + h\nu \rightarrow X^+ + N_1 \quad [2a]$$

$$\rightarrow Y^+ + N_2 \quad [2b]$$

$$\rightarrow Z^+ + N_3 \quad [2c]$$

Action spectra can be acquired for all of the X^+, Y^+ and Z^+ fragment ions where signal intensity allows. An illustrative example is shown in Figure 2, for the protonated form of the sunscreen molecule, octyl methoxy cinnamate (OMC).[38] The photodepletion spectrum of the precursor ion $[OMC{\cdot}H]^+$ is displayed in Figure 2a while Figures 2b-2d display the corresponding photofragment action spectra of the major photofragments with *m/z* 179, 161 and 133. The action spectra of individual PFs can be seen to track the spectral bands evident in the photodepletion spectrum.

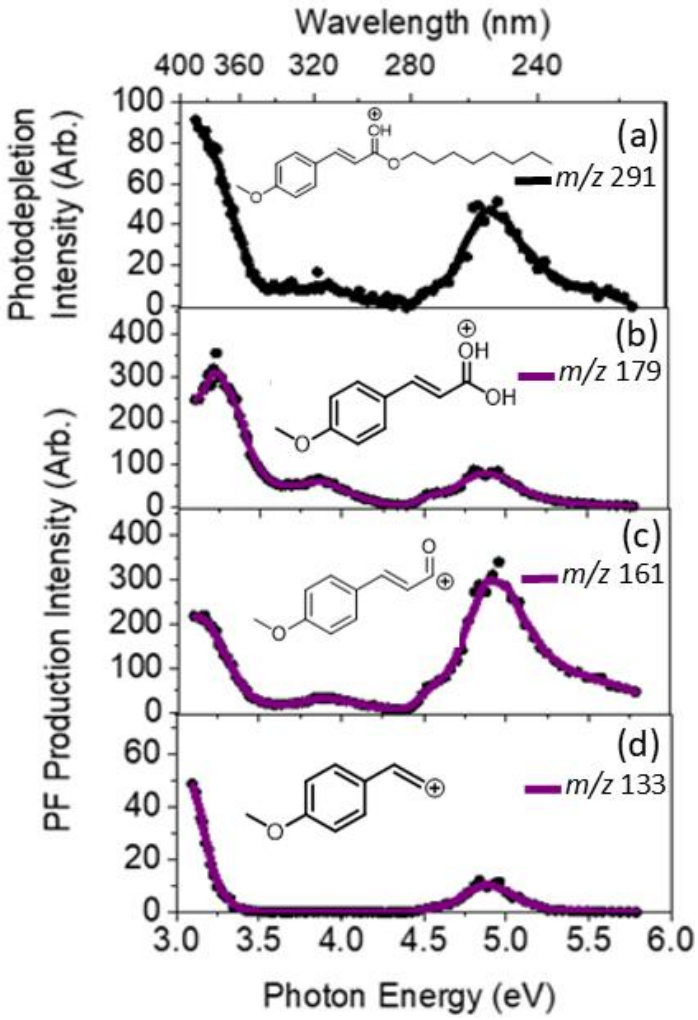

Figure 2: (a) Gas-phase PD (absorption) spectrum of $[OMC+H]^+$, and the complementary photofragment production spectra for the three major PFs with (b) *m/z* 179, (c) *m/z* 161, and (d) *m/z* 133, respectively, with tentative structure assignments included. Adapted from Ref [38]. [38]

Photodepletion and photofragmentation are defined by Equations [3a] and [3b]:

$$\text{Photodepletion (PD) Intensity} = \frac{\text{Ln}\left(\frac{\text{Int}_{OFF}}{\text{Int}_{ON}}\right)}{\lambda \times P} \qquad [3a]$$

$$\text{Photofragmentation (PF) Production} = \frac{\left(\frac{\text{Int}_{Frag}}{\text{Int}_{OFF}}\right)}{\lambda \times P} \qquad [3b]$$

where Int_{ON} and Int_{OFF} are the precursor ion peak intensities with laser on and off, Int_{Frag} is the fragment intensity with laser on, λ is the excitation wavelength (nm) and P is the laser pulse energy (mJ).

Whether the electronic spectrum of $A{\cdot}B^+$ is recorded via PD of the precursor ion or via PF production spectra (individual or summed) depends on signal-to-noise considerations, which vary as a function of instrumental set up, molecular system and absorption intensity across the wavelength range studied. In situations where signal-to-noise is relatively low, it can be necessary to acquire the electronic spectrum by summing all photofragment channels, *i.e.* channels [2a]-[2c] for the M^+ example, into a single action spectrum.[21,22,37]

Electronic action spectroscopy is a widely applicable technique, with only a small number of limitations. One is that detection of charged PFs can sometimes be hampered by a low-mass cut-off, depending on the instrument employed.[39] In general, this is more of a problem when the precursor ion itself has a low *m/z* value since PFs are then more likely to fall below the low-mass cut-off. Secondly, it is important that the excited state decays over a timescale that is shorter than the detection window for the PFs. Finally, action spectra will be perturbed if the ionic excited state decays by fluorescence, since then fragmentation may be reduced. While this may appear a significant limitation, in practice the acquired action spectrum can be compared against the solution-phase UV-VIS absorption spectrum profile to establish whether significant fluorescence is present. It appears that across the very wide number of gaseous ionic systems studied, fluorescence is rare, since the action spectra PD profiles mirroring the solution-phase absorption spectra. (Investigations into the gaseous green fluorescent protein chromophore provide further insight into this topic.[40]) We note that it is possible to acquire fluorescence spectra of gaseous ions for a limited number of systems with strong fluorescence quantum yields.[21,41]

A number of reviews cover electronic (UV-VIS) action spectroscopy of gaseous ions; [8,9,20,22,41,42] providing further details of the technique and its range of application. Sentence deleted as now incorporated into page 4 discussion.

Advantages of Distinguishing Individual Photofragmentation Channels

Once an electronic spectrum is acquired by action spectroscopy, excited states are identified by determining the locations of peaks in the spectral profile, which are broadly assumed to correlate with the experimental vertical excitation energies. This practice is followed whether the overall electronic spectrum is acquired via photodepletion of the precursor ion or via

summing all the observed fragment pathways. A number of issues can, however, hamper this approach.

The first is the generic problem in electronic spectroscopy where bands from different excited states overlap. This situation is frequently encountered in condensed phase UV-VIS, and is equally common in gaseous ion spectroscopy given that ESI generates ions with ambient internal energy ions. (Cryogenic ion spectroscopy offers one solution that can typically improve spectral band resolution,[16,43,44] but it is expensive and technically advanced to implement.) A particularly important problem arises in systems where isomeric structures are present,[45,46] since the isomer contributions will necessarily result in overlapping and potentially unresolved PD spectra.

Resolution of action spectra into individual PF channels can significantly improve spectral congestion issues that arise due to the presence of isomers. A recent example from our laboratory was observed for protonated nicotinamide (NA).[47] Nicotinamide has multiple possible protonation sites, allowing a number of protonation isomers (protomers) to be formed during ESI. The PD (gas-phase absorption) spectrum for protonated nicotinamide, $NA{\cdot}H^+$, is displayed in the left-hand side panel of Figure 3, showing a broad absorption onset above 3.8 eV, a prominent broad band centred around 4.8 eV, and rising photoabsorption towards the high-energy spectral edge. If only the PD spectrum was considered, it would likely lead to the conclusion that the spectrum arises from a single, strong UV excitation centred at 4.8 eV, with a lower-intensity transition in the region of 4.1 eV. (Higher-energy excitations will clearly be present in the UVC region.) However, a very different picture emerges when the action spectra for production of individual PFs are inspected. The right-hand side panel of Figure 3 displays three distinct mass-channel action spectra, corresponding to the spectra for the *m/z* 106, 96 and 80 PFs. Inspection of these spectra shows that a different chromophore is responsible for the PFs that are produced in the Figure 3a and 3b spectra, while the *m/z* 80 (Figure 3c) PF spectrum displays features associated with the two chromophores evident in the *m/z* 106 and 96 spectra. Further analysis revealed that the chromophores present in the Figure 3a and 3b spectra are associated with a carbonyl protomer and a pyridine protomer, respectively.[47] This allowed experimental VEEs for both protomers to be obtained and compared against theoretical predictions, illustrating the advantage of resolving individual PF action spectra.

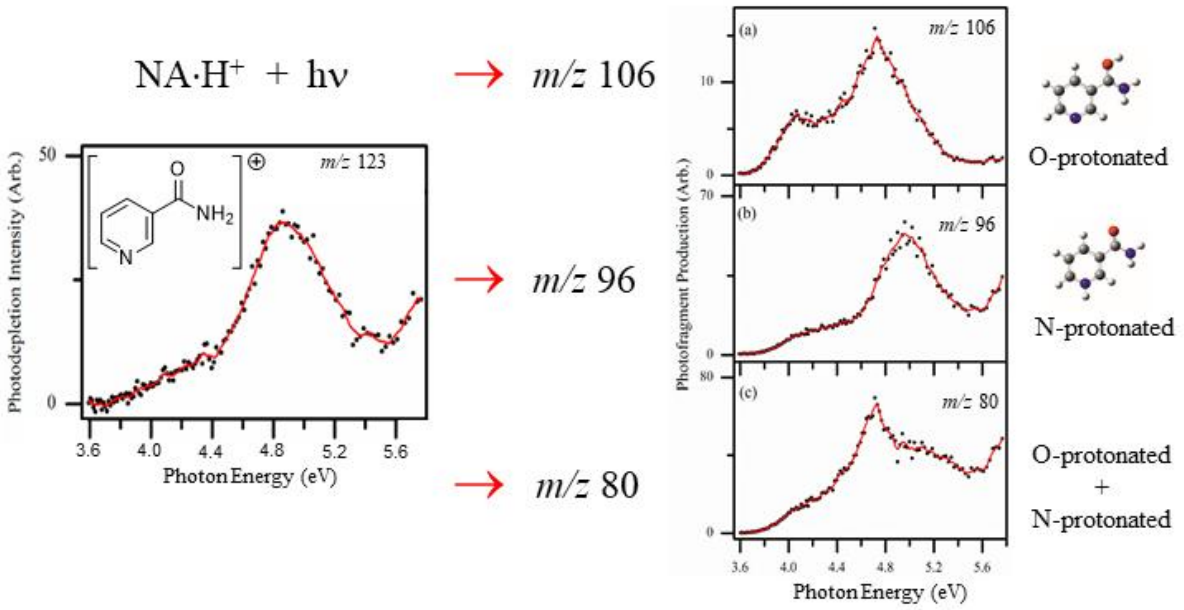

Figure 3: Gas-phase PD spectrum (absorption spectrum) of protonated nicotinamide, NA·H$^+$, across the range 3.6–5.8 eV (left hand side), displayed with the corresponding PF action spectra (right hand side) of the *m/z* = (a) 106, (b) 96, and (c) 80 PFs produced following photoexcitation of mass-selected NA·H$^+$ ions across the range 3.56–5.8 eV. Adapted with permission from Ref [47]. Copyright 2016, American Chemical Society.[47]

Characterising Dissociative Excited States with Relative Ion Yield Plots

In photochemistry, the efficiency of a particular photochemical process is generally described in terms of the quantum yield, which is defined as the number of photochemical events that occur per photon of light absorbed by a molecular system.[48] The quantum yield is used to quantify the extent of photochemical processes including luminescence, photolysis and photochemical bond-formation reactions. A plot of relative quantum yields for the various active processes of a given molecular system therefore provides a concise visual overview of how different photochemical events occur across a range of photoexcitation energies. Our group has recently demonstrated that a similar analysis of ion photodissociation spectroscopy photofragmentation channels provides an overall perspective on PF production as a function of photon energy. In our work, relative ion yields have been calculated according to Equation [4]:

$$\text{Relative Ion Yield} = \frac{Int_{Frag}}{Int_{PFT}} \qquad [4]$$

where Int_{PFT} is the sum of the PF ion intensities obtained with the laser on at a given photon energy.[49] The relative ion yield plots obtained as a function of photon energy strikingly show how PF production is controlled by the morphology of the excited states, and not simply by the molecular internal energy following photoexcitation, *i.e.* photofragmentation does not simply increase as a function of photon energy. Peaks in the relative ion yield plots are then considered to be the locations of the vertical excitation energies.

Presentation of the PF action spectra as relative ion yield plots brings an immediate clarity to the locations of bright electronic excited states. Figure 4 presents an early example, displaying the relative ion yield plots for the deprotonated UV filter molecule 2-phenylbenimidazole-5-sulfonic acid, PBSA.[50] Without embarking on a detailed discussion of the $[PBSA-H]^-$ photofragmentation processes, the relative ion yield plots (RHS Figure 4) reveal the presence of two dominant bright electronic states, associated with peaks in PF production, indicated by the grey bars on the relative ion yield plot: One peaks at 3.77 eV (accompanied by production of the *m/z* 208 and 80 PFs), and a second at 4.55 eV (accompanied by production of PF *m/z* 193).

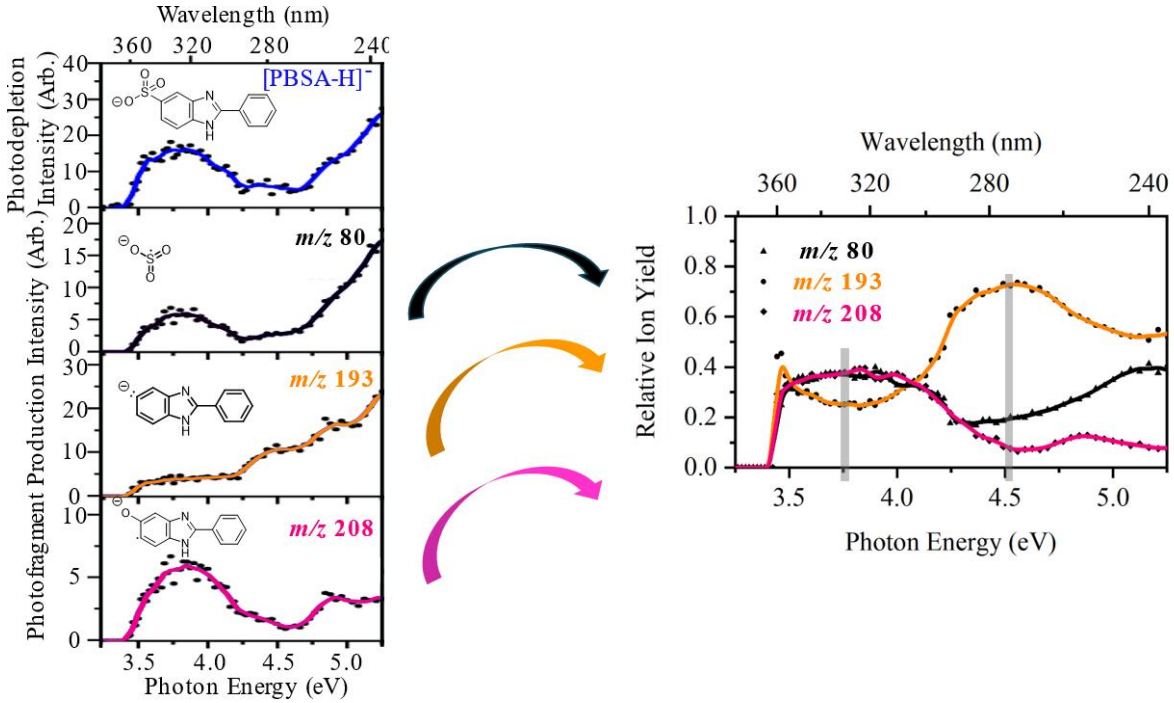

Figure 4: Left hand side (LHS): Gas-phase PD spectrum of $[PBSA-H]^-$ displayed with the corresponding PF action spectra for the m/z 80, 193 and 208 PFs. Right hand side (RHS): Corresponding relative ion yield plots obtained from the PF action spectra. The grey bars indicate the experimental vertical excitation energies. Adapted from Ref [50]. Copyright 2019, Wiley.[50]

Comparison of PF action spectra (LHS Figure 4) and the relative ion yield plots (RHS Figure 4) illustrate the advantages of presenting the data in relative ion yield format. Firstly, although the PF action spectra (LHS Figure 4) have peaks in production around 3.8 eV, it is not obvious that the production intensities of the *m/z* 80 and *m/z* 208 PFs are equally maximised through this region, indicating equivalent photochemical production of these PFs through this excited state region. Most striking is the clear evidence for the location of a second bright state at 4.55 eV, associated with enhanced photochemical production of the PF *m/z* 193. This phenomenon is difficult to discern from the PF action spectra as it is necessary to consider that the intensity of the *m/z* 193 PF is increasing (in particular between 4.25-4.5 eV) while the intensities of the other two PFs are relatively stable. Finally, the relative ion yield plots make clear that a third, less bright excited state is present at 4.80 eV, and is associated solely with production of the *m/z* 208 PF. From the individual PF action spectra, it would not be clear if this state was associated with production of just *m/z* 208 or also with PF *m/z* 193. The relative ion yield analysis removes any ambiguity.

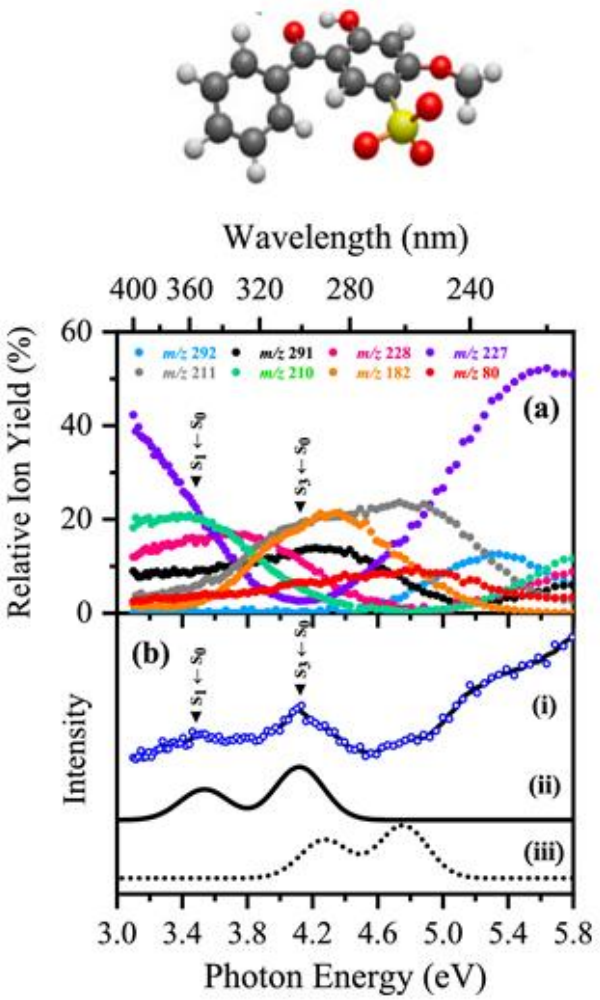

Figure 5: (a) Relative ion yield plot highlighting the eight most intense PFs of [BP4–H]$^-$ (structure displayed at top of figure) for photoexcitation from 3.1-5.8 eV. (b) Gas-phase experimental PD spectrum (i) vs theoretical UV absorption spectra calculated at the (ii) ADC(2)/MP2/ma-*def*2-SV(P) and (iii) ωB97X-D/ma-*def*2-SV(P) levels. The optically bright $S_1 \leftarrow S_0$ and $S_3 \leftarrow S_0$ $\pi\pi^*$ transitions are indicated. Adapted from Ref [51]. License https://creativecommons.org/licenses/by/4.0/. [51]

Although it is possible to argue that the same conclusions could have been reached by a careful inspection of the PF action plots for [PBSA-H]$^-$, ad hoc analysis becomes far more challenging when a molecule photofragments into a greater number of channels. An excellent example is provided by the photochemistry of deprotonated benzophenone-4, [BP4-H]$^-$. Photofragmentation is extensive for this ion, with over 20 PFs being produced across a region from 400-220 nm.[51] The relative ion yield plot for the eight most intense PFs is displayed on Figure 5, along with the gas-phase PD spectrum and theoretical absorption spectra. The ADC(2) S_0-S_1 and S_0-S_3 calculated excited states agree well with two regions of enhanced PF ion production evident in the relative ion yield plot. This system is interesting as comparison of the PFs with the fragments observed upon collisional excitation of the ground state reveals that photoexcitation is being followed by efficient internal conversion back to the electronic ground state, *i.e.* statistical dissociation, which for [BP4-H]$^-$ results in a plethora of ionic fragments.

Finally, we highlight the photodissociation and relative ion yield spectra of the protonated avobenzone system. Avobenzone (AVB) is a classic β-diketone molecule that exists as either a chelated enol or di-keto tautomer (Scheme 1), with the electronic excitations of each isomer being well separated. The photodegradation pathways of AVB were investigated by applying UV photodissociation spectroscopy to protonated AVB ions, *i.e.* [AVB·H]$^+$.[52]

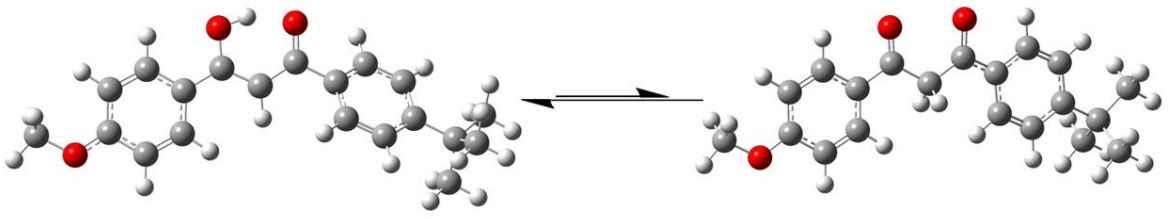

Scheme 1: Schematic diagram of the chelated enol (E) and (di)keto (K) tautomers of avobenzone (AVB). The enol form is the UVA active chromophore, with the keto form being UVB active.

Figure 6 displays the measured total ion yield spectra for $[AVB{\cdot}H]^+$, with Figure 6a displaying the relative ion yield plots for the two major PFs, *m/z* 161 and 135, and Figure 6b displaying those of the secondary PFs, *m/z* 146 and 177.[52] One of the striking aspects of the ion yield spectra is how clearly they reveal which PFs are associated with which AVB isomers: Production of the *m/z* 135 PF peaks strongly at 3.6 and 4.3 eV, energies which coincide with the calculated bright transitions for the primary diketo-tautomer (Figure 6c). Similarly, peaks in the ion yield of the *m/z* 177 PF are aligned with the calculated excitation energies of the chelated enol, Ea isomer. Overall, the close comparison of the PF ion yields with the calculated vertical excitation energies gave detailed information on both the location and identity of the dissociative excited state surfaces of $[AVB{\cdot}H]^+$, and provided new insight into the photodegradation pathways of AVB and the wider class of such β-diketone molecules.

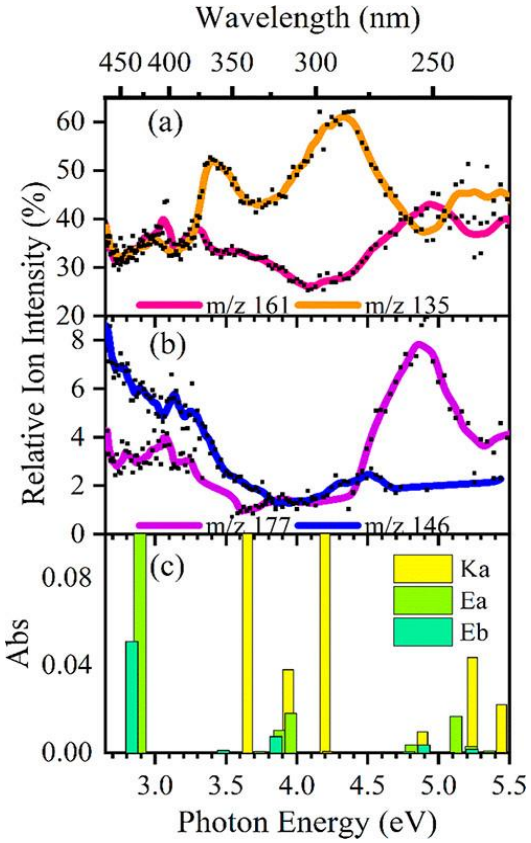

Figure 6: Relative ion yield plots for (a) the *m/z* 161, 135, (b) *m/z* 146, 177 PFs of $AVB{\cdot}H^+$ between 2.6 and 5.5 eV, and (c) the TD-DFT calculated excitation energies for each

isomer at the ωB97X-D/def2-SVP level. Calculated excitation energies have been red-shifted by 0.53 eV. Reproduced from Ref [52] [52]

Summary and Outlook

It is important to emphasise how challenging it remains to a priori predict the way in which a molecule evolves and breaks apart following photoexcitation.[2] A complex set of factors influence the paths followed once electronic excited states are accessed, in particular relating to the changes in molecular geometry that occur across multidimensional potential energy surfaces. These factors make the identification of the reaction channels that lead to photoproducts one of the most problematic areas of computational chemistry, with product prediction only having been achieved to date for a limited number of systems through machine-learning enhanced non-adiabatic molecular dynamics simulations of trained potentials.[53] Gas-phase photodissociation spectroscopy provides a rich source of experimental data on energy-dependent photoproduct production that frontier theoretical calculations can be benchmarked against. Relative ion yield plots have now been obtained for a range of cationic and anionic systems, including organic, inorganic (e.g. manganese and ruthenium metal carbonyls) and biomolecular ions (e.g. riboflavin).[38,50–52,54,55] They reveal direct experimental information on energy-dependent production of photoproducts which can be used to test new theoretical approaches by providing clarity on the locations of experimental VEEs.

In a photochemical context, one of the most useful aspects of relative ion yield plots is that they allow clear identification of photochemical fragments, i.e. ionic fragments that are produced through dissociative excited state surfaces instead of from hot electronic ground states. Deprotonated riboflavin provides an excellent example, where photochemical and non-photochemical ionic fragments are clearly differentiated in the relative ion yield analysis due to the distinctive profiles of photochemical and non-photochemical fragments.[54] Furthermore, ion-yield plots can provide insight into dynamical aspects of excited state behaviour, as demonstrated for the non-native synthetic nucleobase, Z (6-amino-5-nitro-2(1*H*)-pyridone), where the relative ion yield analysis provides exquisite evidence that the molecule undergoes ultrafast excited-state decay with boil off of the OH functional group of Z from the hot electronic ground state.[56]

It is useful, finally, to reflect on the relationship between the gas-phase action spectroscopy measurements detailed here and work by Barner-Kowollik and co-workers on wavelength-resolved photochemical action plots obtained from solution-phase measurements.[57] Their work has uncovered numerous cases where a mismatch exists between the absorption spectrum of a chromophore and the wavelength-resolved photochemical reactivity (associative and dissociative) observed, challenging one of the fundamental paradigms of photochemistry. In our gas-phase measurements, we have observed no such effects for any of the dissociative photochemistry we have studied, suggesting that the effects that Barner-Kowollik and co-workers are observing are not the result of intrinsic photochemical anomalies such as violations of Kasha's law. Intriguingly, they have very recently published a new study where they trace the underlying mechanism behind the mismatched reactivity and absorbance in photocycloadditions to specific microenvironments experienced by the reactive precursors.[58] While some questions may remain about the mechanisms of the effects observed in the solution-phase photochemical action plots, these are clearly important measurements with relevance to a wide range of photo-activated synthesis and materials science. It would be highly valuable to obtain action plots for selected systems via both the gas-phase approach described here as well as the solution-phase action-plot approach. This should provide a deeper insight into the fundamental photochemical and photophysical mechanisms at play in these important chemical systems.

Acknowledgements

Financial support from the EPSRC (EP/X010724/1), Leverhulme Trust (Research Project Grant RPG-2017-147) and European Research Council (208589-BIOIONS) is gratefully acknowledged. CEHD acknowledges conversations with Prof Robin Perutz that inspired the development of the relative ion yield plots.

Conflict of Interest

The authors declare no conflicts of interest.

References

(1) Goti, G.; Manal, K.; Sivaguru, J.; Dell'Amico, L. The Impact of UV Light on Synthetic Photochemistry and Photocatalysis. *Nat. Chem.* **2024**, *16* (5), 684–692. https://doi.org/10.1038/s41557-024-01472-6.
(2) Mai, S.; González, L. Molecular Photochemistry: Recent Developments in Theory. *Angew. Chem. Int. Ed.* **2020**, *59* (39), 16832–16846. https://doi.org/10.1002/anie.201916381.
(3) Duncan, M. A. Frontiers in the Spectroscopy of Mass-Selected Molecular Ions. *Int. J. Mass Spectrom.* **2000**, *200* (1), 545–569. https://doi.org/10.1016/S1387-3806(00)00366-3.
(4) Brutschy, B.; Hobza, P. Van Der Waals Molecules III: Introduction. *Chem. Rev.* **2000**, *100* (11), 3861–3862. https://doi.org/10.1021/cr990074x.
(5) Vries, M. S. de; Hobza, P. Gas-Phase Spectroscopy of Biomolecular Building Blocks. *Annu. Rev. Phys. Chem.* **2007**, *58* (Volume 58, 2007), 585–612. https://doi.org/10.1146/annurev.physchem.57.032905.104722.
(6) Dessent, C. E. H.; Müller-Dethlefs, K. Hydrogen-Bonding and van Der Waals Complexes Studied by ZEKE and REMPI Spectroscopy. *Chem. Rev.* **2000**, *100* (11), 3999–4022. https://doi.org/10.1021/cr990060r.
(7) Bieske, E. J. Spectroscopic Studies of Anion Complexes and Clusters: A Microscopic Approach to Understanding Anion Solvation. *Chem. Soc. Rev.* **2003**, *32* (4), 231–237. https://doi.org/10.1039/B106752B.
(8) Antoine, R.; Dugourd, P. Visible and Ultraviolet Spectroscopy of Gas Phase Protein Ions. *Phys. Chem. Chem. Phys.* **2011**, *13* (37), 16494–16509. https://doi.org/10.1039/C1CP21531K.
(9) Rizzo, T. R.; Stearns, J. A.; Boyarkin, O. V. Spectroscopic Studies of Cold, Gas-Phase Biomolecular Ions. *Int. Rev. Phys. Chem.* **2009**, *28* (3), 481–515. https://doi.org/10.1080/01442350903069931.
(10) Hamouda, R.; Bellina, B.; Bertorelle, F.; Compagnon, I.; Antoine, R.; Broyer, M.; Rayane, D.; Dugourd, P. Electron Emission of Gas-Phase [Au25(SG)18-6H]7− Gold Cluster and Its Action Spectroscopy. *J. Phys. Chem. Lett.* **2010**, *1* (21), 3189–3194. https://doi.org/10.1021/jz101287m.
(11) Harville, P. A.; Moss, O. C.; Rana, A.; Snowden, E. A.; Johnson, M. A. Demonstration of Capture, Cooling, Tagging, and Spectroscopic Characterization of UV Photoproduct Ions in a Cryogenic Ion Trap: Application to 266 Nm Photofragment Ions from Rhodamine 6G. *J. Phys. Chem. A* **2024**, *128* (36), 7714–7719. https://doi.org/10.1021/acs.jpca.4c04283.
(12) Navrátil, R.; Jašík, J.; Roithová, J. Visible Photodissociation Spectra of Gaseous Rhodamine Ions: Effects of Temperature and Tagging. *J. Mol. Spectrosc.* **2017**, *332*, 52–58. https://doi.org/10.1016/j.jms.2016.10.016.
(13) Nielsen, S. B.; Lapierre, A.; Andersen, J. U.; Pedersen, U. V.; Tomita, S.; Andersen, L. H. Absorption Spectrum of the Green Fluorescent Protein Chromophore Anion In Vacuo. *Phys. Rev. Lett.* **2001**, *87* (22), 228102. https://doi.org/10.1103/PhysRevLett.87.228102.
(14) Kjær, C.; Bull, J. N.; Carrascosa, E.; Nielsen, S. B.; Bieske, E. J. Action Spectroscopy of Isomer-Selected Luciferin Anions. *Eur. Phys. J. D* **2021**, *75* (3), 72. https://doi.org/10.1140/epjd/s10053-021-00076-w.
(15) Jin, S.; Juanes, M.; Reimann, M.; van der Linde, C.; Ončák, M.; Beyer, M. K. The UV Photodissociation Spectrum of FeOH+: Electronic Insight into the Simplest Iron Hydroxide Complexes. *J. Phys. Chem. A* **2025**. https://doi.org/10.1021/acs.jpca.5c06546.
(16) Zagorec-Marks, W.; Dodson, L. G.; Weis, P.; Schneider, E. K.; Kappes, M. M.; Weber, J. M. Intrinsic Structure and Electronic Spectrum of Deprotonated Biliverdin: Cryogenic Ion Spectroscopy and Ion Mobility. *J. Am. Chem. Soc.* **2021**, *143* (42), 17778–17785. https://doi.org/10.1021/jacs.1c08701.
(17) Noble, J. A.; Marceca, E.; Dedonder, C.; Carvin, I.; Gloaguen, E.; Jouvet, C. Photofragmentation and Electron Detachment of Aromatic Phosphonate, Sulfonate and Phosphate Oxyanions. *Eur. Phys. J. D* **2021**, *75* (3), 95. https://doi.org/10.1140/epjd/s10053-021-00094-8.

(18) Eun, H. J.; Ishiuchi, S.; Yoo, I. T.; Heo, J.; Park, J. W.; Fujii, M.; Kim, N. J. Cryogenic Ion Spectroscopy of Protonated and Sodiated Methyladenine Derivatives. *J. Phys. Chem. A* **2023**, *127* (11), 2472–2480. https://doi.org/10.1021/acs.jpca.2c09083.
(19) Studemund, T.; Pollow, K.; Förstel, M.; Dopfer, O. Photochemical Properties of a Potential Interstellar Dust Precursor: The Electronic Spectrum of Si3O2+. *Phys. Chem. Chem. Phys.* **2023**, *25* (26), 17609–17618. https://doi.org/10.1039/D3CP02693K.
(20) Tureček, F. UV-vis Spectroscopy of Gas-phase Ions. *Mass Spectrom. Rev.* **2023**, *42* (1), 206–226. https://doi.org/10.1002/mas.21726.
(21) Stockett, M. H.; Houmøller, J.; Støchkel, K.; Svendsen, A.; Brøndsted Nielsen, S. A Cylindrical Quadrupole Ion Trap in Combination with an Electrospray Ion Source for Gas-Phase Luminescence and Absorption Spectroscopy. *Rev. Sci. Instrum.* **2016**, *87* (5), 053103. https://doi.org/10.1063/1.4948316.
(22) Marlton, S. J. P.; Trevitt, A. J. The Combination of Laser Photodissociation, Action Spectroscopy, and Mass Spectrometry to Identify and Separate Isomers. *Chem. Commun.* **2022**, *58* (68), 9451–9467. https://doi.org/10.1039/D2CC02101C.
(23) Razmus, W. O.; Allum, F.; Harries, J.; Kumagai, Y.; Nagaya, K.; Bhattacharyya, S.; Britton, M.; Brouard, M.; Bucksbaum, P. H.; Cheung, K.; Crane, S. W.; Fushitani, M.; Gabalski, I.; Gejo, T.; Ghrist, A.; Heathcote, D.; Hikosaka, Y.; Hishikawa, A.; Hockett, P.; Jones, E.; Kukk, E.; Iwayama, H.; Lam, H. V. S.; McManus, J. W.; Milesevic, D.; Mikosch, J.; Minemoto, S.; Niozu, A.; Orr-Ewing, A. J.; Owada, S.; Rolles, D.; Rudenko, A.; Townsend, D.; Ueda, K.; Unwin, J.; Vallance, C.; Venkatachalam, A.; Wada, S.; Walmsley, T.; Warne, E. M.; Woodhouse, J. L.; Burt, M.; Ashfold, M. N. R.; Minns, R. S.; Forbes, R. Exploring the Ultrafast and Isomer-Dependent Photodissociation of Iodothiophenes via Site-Selective Ionization. *Phys. Chem. Chem. Phys.* **2024**, *26* (16), 12725–12737. https://doi.org/10.1039/D3CP06079A.
(24) Baker, L. A.; Horbury, M. D.; Greenough, S. E.; Coulter, P. M.; Karsili, T. N. V.; Roberts, G. M.; Orr-Ewing, A. J.; Ashfold, M. N. R.; Stavros, V. G. Probing the Ultrafast Energy Dissipation Mechanism of the Sunscreen Oxybenzone after UVA Irradiation. *J. Phys. Chem. Lett.* **2015**, *6* (8), 1363–1368. https://doi.org/10.1021/acs.jpclett.5b00417.
(25) Livingstone, R. A.; Thompson, J. O. F.; Iljina, M.; Donaldson, R. J.; Sussman, B. J.; Paterson, M. J.; Townsend, D. Time-Resolved Photoelectron Imaging of Excited State Relaxation Dynamics in Phenol, Catechol, Resorcinol, and Hydroquinone. *J. Chem. Phys.* **2012**, *137* (18), 184304. https://doi.org/10.1063/1.4765104.
(26) Holt, E. L.; Rodrigues, N. d N.; Cebrián, J.; Stavros, V. G. Determining the Photostability of Avobenzone in Sunscreen Formulation Models Using Ultrafast Spectroscopy. *Phys. Chem. Chem. Phys.* **2021**, *23* (42), 24439–24448. https://doi.org/10.1039/D1CP03610F.
(27) Dean, J. C.; Kusaka, R.; Walsh, P. S.; Allais, F.; Zwier, T. S. Plant Sunscreens in the UV-B: Ultraviolet Spectroscopy of Jet-Cooled Sinapoyl Malate, Sinapic Acid, and Sinapate Ester Derivatives. *J. Am. Chem. Soc.* **2014**, *136* (42), 14780–14795. https://doi.org/10.1021/ja5059026.
(28) Romanov, I.; Boeije, Y.; Toldo, J. M.; Do Casal, M. T.; Barbatti, M.; Buma, W. J. Spectroscopy and Excited-State Dynamics of Methyl Ferulate in Molecular Beams. *J. Phys. Chem. A* **2025**, *129* (1), 36–49. https://doi.org/10.1021/acs.jpca.4c05792.
(29) Iida, Y.; Kinoshita, S.; Kenjo, S.; Muramatsu, S.; Inokuchi, Y.; Zhu, C.; Ebata, T. Electronic States and Nonradiative Decay of Cold Gas-Phase Cinnamic Acid Derivatives Studied by Laser Spectroscopy with a Laser-Ablation Technique. *J. Phys. Chem. A* **2020**, *124* (27), 5580–5589. https://doi.org/10.1021/acs.jpca.0c03646.
(30) Boyarkin, O. V.; Mercier, S. R.; Kamariotis, A.; Rizzo, T. R. Electronic Spectroscopy of Cold, Protonated Tryptophan and Tyrosine. *J. Am. Chem. Soc.* **2006**, *128* (9), 2816–2817. https://doi.org/10.1021/ja058383u.
(31) Sen, A.; Bouchet, A.; Lepère, V.; Le Barbu-Debus, K.; Scuderi, D.; Piuzzi, F.; Zehnacker-Rentien, A. Conformational Analysis of Quinine and Its Pseudo Enantiomer Quinidine: A Combined Jet-

Cooled Spectroscopy and Vibrational Circular Dichroism Study. *J. Phys. Chem. A* **2012**, *116* (32), 8334–8344. https://doi.org/10.1021/jp3047888.
(32) Wang, X.-B.; Wang, L.-S. Photoelectron Spectroscopy of Multiply Charged Anions. *Annu. Rev. Phys. Chem.* **2009**, *60* (Volume 60, 2009), 105–126. https://doi.org/10.1146/annurev.physchem.59.032607.093724.
(33) Bradforth, S. E.; Kim, E. H.; Arnold, D. W.; Neumark, D. M. Photoelectron Spectroscopy of CN−, NCO−, and NCS−. *J. Chem. Phys.* **1993**, *98* (2), 800–810. https://doi.org/10.1063/1.464244.
(34) Henley, A.; Fielding, H. H. Anion Photoelectron Spectroscopy of Protein Chromophores. *Int. Rev. Phys. Chem.* **2019**, *38* (1), 1–34. https://doi.org/10.1080/0144235X.2018.1548807.
(35) Anstöter, C. S.; Curchod, B. F. E.; Verlet, J. R. R. Geometric and Electronic Structure Probed along the Isomerisation Coordinate of a Photoactive Yellow Protein Chromophore. *Nat. Commun.* **2020**, *11* (1), 2827. https://doi.org/10.1038/s41467-020-16667-x.
(36) Pereverzev, A.; Roithová, J. Experimental Techniques and Terminology in Gas-Phase Ion Spectroscopy. *J. Mass Spectrom.* **2022**, *57* (5), e4826. https://doi.org/10.1002/jms.4826.
(37) Dang, A.; Korn, J. A.; Gladden, J.; Mozzone, B.; Tureček, F. UV–Vis Photodissociation Action Spectroscopy on Thermo LTQ-XL ETD and Bruker amaZon Ion Trap Mass Spectrometers: A Practical Guide. *J. Am. Soc. Mass Spectrom.* **2019**, *30* (9), 1558–1564. https://doi.org/10.1007/s13361-019-02229-z.
(38) Wong, N. G. K.; Sereli, M.; Anstöter, C. S.; Dessent, C. E. H. Photochemical Degradation of the UV Filter Octyl Methoxy Cinnamate Probed via Laser-Interfaced Mass Spectrometry. *Molecules* **2022**, *27* (24), 8796. https://doi.org/10.3390/molecules27248796.
(39) Berden, G.; Derksen, M.; Houthuijs, K. J.; Martens, J.; Oomens, J. An Automatic Variable Laser Attenuator for IRMPD Spectroscopy and Analysis of Power-Dependence in Fragmentation Spectra. *Int. J. Mass Spectrom.* **2019**, *443*, 1–8. https://doi.org/10.1016/j.ijms.2019.05.013.
(40) Lindkvist, T. T. Turning on the Fluorescence from Isolated GFP Chromophore Anions at Cryogenic Temperatures. *Phys. Rev. Lett.* **2025**, *134* (9). https://doi.org/10.1103/PhysRevLett.134.093001.
(41) Bian, Q.; Forbes, M. W.; Talbot, F. O.; Jockusch, R. A. Gas-Phase Fluorescence Excitation and Emission Spectroscopy of Mass-Selected Trapped Molecular Ions. *Phys. Chem. Chem. Phys.* **2010**, *12* (11), 2590–2598. https://doi.org/10.1039/B921076H.
(42) Andersen, J. U.; Hvelplund, P.; Nielsen, S. B.; Tomita, S.; Wahlgreen, H.; Møller, S. P.; Pedersen, U. V.; Forster, J. S.; Jørgensen, T. J. D. The Combination of an Electrospray Ion Source and an Electrostatic Storage Ring for Lifetime and Spectroscopy Experiments on Biomolecules. *Rev. Sci. Instrum.* **2002**, *73* (3), 1284–1287. https://doi.org/10.1063/1.1447305.
(43) Ohara, S.; Hirata, K.; Grégoire, G.; Fujii, M.; Dopfer, O.; Ishiuchi, S. Optical and Infrared Spectroscopy of Lumiflavin Protomers in a Cryogenic Ion Trap. *J. Phys. Chem. A* **2025**, *129* (24), 5245–5250. https://doi.org/10.1021/acs.jpca.5c01350.
(44) Wolk, A. B.; Leavitt, C. M.; Garand, E.; Johnson, M. A. Cryogenic Ion Chemistry and Spectroscopy. *Acc. Chem. Res.* **2014**, *47* (1), 202–210. https://doi.org/10.1021/ar400125a.
(45) Matthews, E.; Cercola, R.; Dessent, C. E. H. Protomer-Dependent Electronic Spectroscopy and Photochemistry of the Model Flavin Chromophore Alloxazine. *Molecules* **2018**, *23* (8), 2036. https://doi.org/10.3390/molecules23082036.
(46) Uleanya, K. O.; Cercola, R.; Nikolova, M.; Matthews, E.; Wong, N. G. K.; Dessent, C. E. H. Observation of Enhanced Dissociative Photochemistry in the Non-Native Nucleobase 2-Thiouracil. *Molecules* **2020**, *25* (14), 3157. https://doi.org/10.3390/molecules25143157.
(47) Matthews, E.; Dessent, C. E. H. Locating the Proton in Nicotinamide Protomers via Low-Resolution UV Action Spectroscopy of Electrosprayed Solutions. *J. Phys. Chem. A* **2016**, *120* (46), 9209–9216. https://doi.org/10.1021/acs.jpca.6b10433.
(48) Braslavsky, S. E. Glossary of Terms Used in Photochemistry, 3rd Edition (IUPAC Recommendations 2006). *Pure Appl. Chem.* **2007**, *79* (3), 293–465. https://doi.org/10.1351/pac200779030293.

(49) Cercola, R.; Fischer, K. C.; Sherman, S. L.; Garand, E.; Wong, N. G. K.; Hammerback, L. A.; Lynam, J. M.; Fairlamb, I. J. S.; Dessent, C. E. H. Direct Measurement of the Visible to UV Photodissociation Processes for the PhotoCORM TryptoCORM. *Chem. – Eur. J.* **2020**, *26* (45), 10297–10306. https://doi.org/10.1002/chem.202001077.
(50) Wong, N. G. K.; Berenbeim, J. A.; Dessent, C. E. H. Direct Observation of Photochemical Free Radical Production from the Sunscreen 2-Phenylbenzimidazole-5-Sulfonic Acid via Laser-Interfaced Mass Spectrometry. *ChemPhotoChem* **2019**, *3* (12), 1231–1237. https://doi.org/10.1002/cptc.201900149.
(51) Wong, N. G. K.; Rankine, C. D.; Dessent, C. E. H. Linking Electronic Relaxation Dynamics and Ionic Photofragmentation Patterns for the Deprotonated UV Filter Benzophenone-4. *J. Phys. Chem. Lett.* **2021**, *12* (11), 2831–2836. https://doi.org/10.1021/acs.jpclett.1c00423.
(52) Berenbeim, J. A.; Wong, N. G. K.; Cockett, M. C. R.; Berden, G.; Oomens, J.; Rijs, A. M.; Dessent, C. E. H. Unravelling the Keto–Enol Tautomer Dependent Photochemistry and Degradation Pathways of the Protonated UVA Filter Avobenzone. *J. Phys. Chem. A* **2020**, *124* (15), 2919–2930. https://doi.org/10.1021/acs.jpca.0c01295.
(53) Li, J.; Vacher, M.; Dral, P. O.; Lopez, S. A. Chapter 6 - Machine Learning Methods in Photochemistry and Photophysics. In *Theoretical and Computational Photochemistry*; García-Iriepa, C., Marazzi, M., Eds.; Elsevier, 2023; pp 163–189. https://doi.org/10.1016/B978-0-323-91738-4.00002-6.
(54) Wong, N. G. K.; Rhodes, C.; Dessent, C. Photodegradation of Riboflavin under Alkaline Conditions: What Can Gas-Phase Photolysis Tell Us about What Happens in Solution? *Mol. Basel Switz.* **2021**, *26*. https://doi.org/10.3390/molecules26196009.
(55) Cercola, R.; Wong, N. G. K.; Rhodes, C.; Olijnyk, L.; Mistry, N. S.; Hall, L. M.; Berenbeim, J. A.; Lynam, J. M.; Dessent, C. E. H. A "One Pot" Mass Spectrometry Technique for Characterizing Solution- and Gas-Phase Photochemical Reactions by Electrospray Mass Spectrometry. *RSC Adv.* **2021**, *11* (32), 19500–19507. https://doi.org/10.1039/D1RA02581C.
(56) Whitaker, W.; Moncrieff, K. E.; Anstöter, C. S.; Wong, N. G. K.; Berenbeim, J. A.; Dessent, C. E. H. Probing the Electronic Relaxation Pathways and Photostability of the Synthetic Nucleobase Z via Laser Interfaced Mass Spectrometry. *Phys. Chem. Chem. Phys.* **2022**, *24* (45), 27836–27846. https://doi.org/10.1039/D2CP03831E.
(57) Irshadeen, I. M.; Walden, S. L.; Wegener, M.; Truong, V. X.; Frisch, H.; Blinco, J. P.; Barner-Kowollik, C. Action Plots in Action: In-Depth Insights into Photochemical Reactivity. *J. Am. Chem. Soc.* **2021**, *143* (50), 21113–21126. https://doi.org/10.1021/jacs.1c09419.
(58) Carroll, J. A.; Pashley-Johnson, F.; Klein, M.; Stephan, T.; Pandey, A. K.; Walter, M.; Unterreiner, A.-N.; Barner-Kowollik, C. Microenvironments as an Explanation for the Mismatch between Photochemical Absorptivity and Reactivity. *J. Am. Chem. Soc.* **2025**, *147* (30), 26643–26651. https://doi.org/10.1021/jacs.5c06961.